FATIGUE BEHAVIOUR OF STRUCTURAL STEELS. COMPARISON OF STRAIN-LIFE AND FATIGUE CRACK PROPAGATION DATA

COMPORTAMENTO À FADIGA DE AÇOS ESTRUTURAIS. RELAÇÕES DEFORMAÇÃO-VIDA E TAXAS DE PROPAGAÇÃO DE FENDAS DE FADIGA

D. Carvalho [1], A. L. L. Silva [2,3], A. M. P. Jesus [1,3], A. A. Fernandes[2,3]

[1] Universidade de Trás-os-Montes e Alto Douro, UTAD, Vila Real, Portugal
[2] Faculdade de Engenharia da Universidade do Porto, Porto, Portugal
[3] IDMEC, Porto, Portugal




ABSTRACT

The fatigue behaviours of S235, S355 and S690 structural steel grades have been investigated by means of smooth and compact tension (CT) specimens. Strain-life, cyclic elastoplastic and fatigue crack propagation behaviours are compared for the proposed steels aiming the investigation of the influence of the materials static strength on fatigue. The paper also addresses the mean stress effects on fatigue crack propagation rates, through tests performed for distinct stress ratios. Besides the materials comparison based on pure mode I fatigue crack propagation tests, mixed I/II mode fatigue crack propagation test results are also presented and discussed specifically for the S235 steel grade, using a modified CT specimen. The experimentally observed crack paths on modified CT specimens were simulated by means of the FEM, to assess the history of the mode I and mode II stress intensity factors. The Virtual Crack Closure Technique was applied. The validity of existing models for fatigue crack propagation under mixed-mode conditions were assessed for the S235 steel grade.

RESUMO

Neste artigo são comparados os comportamentos à fadiga dos aços estruturais S235, S355 e S690 recorrendo a ensaios de fadiga de provetes lisos e provetes CT. Procura-se avaliar a influência da resistência estática dos aços na resposta deformação-vida, comportamento elasto-plástico cíclico e nas taxas de propagação de fendas de fadiga. Este trabalho também investiga o efeito da razão de tensões nas taxas de propagação de fendas de fadiga. Para além de ensaios de propagação de fendas de fadiga em modo I puro também são realizados ensaios em modo misto I+II, para o aço S235, usando uma versão modificada do provete CT. As trajetórias das fendas de fadiga medidas experimentalmente são simuladas por elementos finitos e, usando a técnica do fecho de fenda virtual, resulta a história dos fatores de intensidade de tensões em modo I e II. A validade de modelos de propagação de fendas de fadiga em modo misto é testada para o aço S235.

1. INTRODUCTION

The use of high strength structural steels is becoming more frequent since these materials permit light and slender aesthetic structural designs. Despite the significant advantage of the higher static strength of the

high strength structural steels, the fatigue performance of these materials does not increase proportionally to the static strength. Recently, De Jesus *et al.* (2012) demonstrated that the S690 structural steel grade exhibits higher fatigue crack growth rates than the S355 steel, which may lead to reduced fatigue strengths when fatigue crack propagation is the dominant phenomena (e.g. welded details). This paper extends the referred study to a wider range of structural steels, namely to the S235 steel. Also, tests are repeated for another sample of S355 steel to allow the verification of the previous published results by De Jesus *et al.* (2012). Therefore, this paper compares the fatigue behaviour of three structural steel grades based on results of an experimental program of fatigue tests of smooth specimens (ASTM E606) and fatigue crack propagation tests (ASTM E647). Besides this comparison exercise, the S235 structural steel is tested under mixed I+II mode fatigue crack propagation conditions allowing the assessment of mixed-mode fatigue crack propagation relations.

2. OVERVIEW OF FATIGUE APPROACHES

Fatigue approaches may be classed into S–N, local and Fracture Mechanics based approaches. S–N approaches are the basis of current design codes such as the Eurocode 3, part 1-9 (CEN, 2003). This is a global approach that relates the stress range (e.g. nominal, structural or geometric) applied to the component with the fatigue life. With respect to the Eurocode 3, Part 1-9, no distinction is made between procedures for welded and non-welded components. These procedures do not account for the material influence which could be considered a limitation for non-welded components. The application of the S-N approaches for complex geometric details under complex loading conditions could be challenging since the selection of the detail category and the evaluation of required stresses are not straightforward tasks.

Local approaches to fatigue and Fracture Mechanics can be used as alternatives to the global S–N approaches, which requires the knowledge of the fatigue properties of the base materials. The local approaches, recognizing the localized nature of the fatigue damage, propose the correlation of a local damage parameter (e.g. stress, strain, energy) with the number of cycles required to initiate a macroscopic crack. The most well-known relations in this area are the proposals by Basquin (1910), Eq. (1), Coffin (1954) and Manson (1954), Eq. (2), and Morrow (1965), Eq. (3):

$$\frac{\Delta\sigma}{2} = \sigma'_f (2N_f)^b \tag{1}$$

$$\frac{\Delta\varepsilon^P}{2} = \varepsilon'_f (2N_f)^c \tag{2}$$

$$\frac{\Delta\varepsilon}{2} = \frac{\Delta\varepsilon^E}{2} + \frac{\Delta\varepsilon^P}{2} = \\ = \frac{\sigma'_f}{E}(2N_f)^b + \varepsilon'_f (2N_f)^c \tag{3}$$

where σ'_f and b are, respectively, the fatigue strength coefficient and exponent; ε'_f and c are, respectively, the fatigue ductility coefficient and exponent; $2N_f$ is the number of reversals to failure; $\Delta\varepsilon$, $\Delta\varepsilon^E$ and $\Delta\varepsilon^P$ are, respectively, the total, elastic and plastic strain ranges; $\Delta\sigma$ is the stress range and E is the Young's modulus. The constants in these relations may be determined from fatigue tests of smooth specimens under strain-controlled conditions. These tests also allow the identification of the cyclic curve of the material which relates the stress amplitude with the strain amplitude, corresponding to the stabilized behaviour of the material. This relation is usually expressed using the Ramberg–Osgood equation (Ramberg and Osgood, 1943):

$$\frac{\Delta\varepsilon}{2} = \frac{\Delta\varepsilon^E}{2} + \frac{\Delta\varepsilon^P}{2} = \frac{\Delta\sigma}{2E} + \left(\frac{\Delta\sigma}{2K'}\right)^{1/n'} \tag{4}$$

K' and n' are, respectively, the strain hardening coefficient and exponent.

Fracture Mechanics may be also used as an alternative approach to fatigue. Within this approach, fatigue damage corresponds to the fatigue crack propagation. This

approach may be used to complement the local approaches to fatigue (Chen *et al.*, 2005, 2007) allowing the residual life computation of a structural component with an initial defect. This approach is based on crack propagation laws, the Paris's law (Paris and Erdogan, 1963) being one of the most used:

$$da/dN = C(\Delta K)^m \quad (5)$$

where da/dN is the fatigue crack growth rate, ΔK is the stress intensity factor range, C and m are material constants . The number of cycles spent until failure may be computed integrating the crack propagation law between an initial crack size (a_i) and a critical crack size (a_f):

$$N_f = \int_{a_i}^{a_f} \frac{da}{C(\Delta K)^m} \quad (6)$$

Both local and Fracture Mechanics approaches need the materials characterization by means of fatigue tests of smooth specimens and fatigue crack propagation tests. These tests are required to compute the constants of Equations (1) to (5). The referred tests will be the basis for the comparison of the fatigue behaviour between the three structural steels under investigation.

3. MATERIALS AND EXPERIMENTAL DETAILS

A comparison of the fatigue properties between the S235, S355 and S690 structural steels is proposed in this research. These steel grades are specified according to the EN10025 standard (CEN, 2004). Minimum yield stresses of 235, 355 and 690 MPa are specified, respectively, for the S235, S355 and S690 steel grades, for nominal thicknesses below 16 mm. The tensile strengths fall within the ranges 360-510MPa, 470-630MPa and 770-940MPa respectively for S235, S355 and S690 steels. Comparing the yield strengths, the S355 steel exhibits nominal yield strength 120 MPa higher than S235 steel. The S690 shows a yield strength 335MPa higher than S355 steel grade, representing almost twice the yield strength of the S355 steel grade. While S690 steel is considered a high strength steel, the S355 and S235 steels are considered mild steels.

Fatigue tests on smooth specimens were carried out according the ASTM E606 standard (ASTM, 1998), under strain controlled conditions. In addition, fatigue crack propagation tests were performed using compact tension (CT) specimens, in accordance with the procedures of the ASTM E647 standard (ASTM, 1999), under load controlled conditions. In this work, only the S235 and S355 steels were tested, but similar test results were performed in a previous work by De Jesus *et al.* (2012) covering the S355 and S690 steel grades, which will be referred in this paper for comparison purposes. All the referred tests were performed, at room temperature and in air, in a close-loop servohydraulic INSTRON 8801 machine, rated to 100kN.

Fig. 1 shows the general geometry of the smooth specimens and Table 1 specifies the dimensions adopted for each steel grade. Distinct sizes of specimens were considered for each steel grade, since specimens were extracted from plates with different thicknesses. Nevertheless, the geometries are in accordance with the ASTM E606 recommendation. The gauge length of the specimens was polished with an appropriate sequence of sandpapers. The strain was controlled using an INSTRON 2620-202 dynamic clip gauge, with a range of ±2.5 mm.

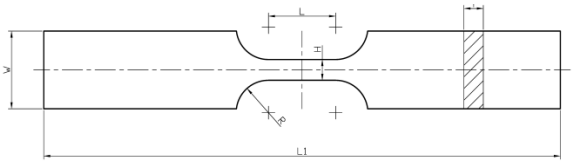

Fig. 1 – Geometry of the smooth plane specimens.

Tab. 1 – Dimensions of the smooth plane specimens.

Material	*W* mm	*T* mm	*L* mm	*L1* mm	*H* mm	*R* mm
S235*	20	5	15	135	6	12
S355*	20	5	15	100	6	12
S355**	30	7.5	26	200	12.5	8
S690**	16	4	13	110	8	4.5

*Tested in this study

**Tested by De Jesus *et al.* (2012)

All tests were instrumented with a reference gauge length of 12.5 mm except the specimens made of S355 steel and tested by De Jesus *et al.* (2012) that were instrumented with a reference gauge length of 25 mm. The fatigue tests of smooth specimens performed in this work were conducted for a strain ratio, R_ε, equal to 0, following a sinusoidal waveform with a frequency adjusted to result an average strain rate of 0.8%/s. Tests performed by the De Jesus *et al.* (2012) were conducted with R_ε=–1.

Table 2 and Table 3 summarize the tests performed in this work and the applied strain ranges, including the plastic and elastic components which were assessed for the stabilized cyclic behaviour.

Concerning the fatigue crack propagation tests, Fig. 2 and Table 4 summarizes the geometries and dimensions of the standard specimens. In this study, two distinct thicknesses for the S355 steel were tested, namely with B=4 and B=8 mm. Besides the standard CT specimens, modified CT specimens were also tested for the S235 steel. The modified CT specimens were provided with an extra circular side hole in order to generate deviations from the pure mode I fatigue crack propagation (see Fig. 3). These specimens will be used to generate mixed-mode fatigue crack propagation conditions for the S235 steel. This modified CT geometry shows the same base geometry of the CT specimen used for the S235 steel.

Tab. 2 – Summary of the fatigue tests performed on smooth specimens made of S235 steel.

Specimens	$\Delta\varepsilon$ [%]	$\Delta\varepsilon^P$ [%]	$\Delta\varepsilon^E$ [%]
S235-100-01	1.00	0.63	0.37
S235-100-02	1.00	0.65	0.35
S235-200-01	2.00	1.55	0.45
S235-200-02	2.00	1.57	0.43
S235-050-01	0.50	0.20	0.30
S235-050-02	0.50	0.19	0.31
S235-040-01	0.40	0.08	0.32
S235-040-02	0.40	0.11	0.29
S235-030-01	0.30	0.04	0.26
S235-040-03	0.40	0.11	0.29
S235-030-02	0.30	0.03	0.27
S235-025-01	0.25	0.00	0.25

Tab. 3 – Summary of the fatigue tests performed on smooth specimens made of S355 steel.

Specimens	$\Delta\varepsilon$ [%]	$\Delta\varepsilon^P$ [%]	$\Delta\varepsilon^E$ [%]
S355-200-01	2.00	1.53	0.47
S355-100-01	1.00	0.60	0.40
S355-200-02	2.00	1.53	0.47
S355-100-02	1.00	0.62	0.38
S355-0.50-01	0.50	0.21	0.29
S355-0.50-02	0.50	0.20	0.30
S355-0.40-01	0.40	0.14	0.26
S355-0.40-02	0.40	0.13	0.27
S355-0.30-01	0.30	0.06	0.24
S355-0.30-02	0.30	0.01	0.29
S355-0.25-01	0.25	0.02	0.23
S355-0.75-01	0.75	0.40	0.35
S355-0.75-02	0.75	0.40	0.35

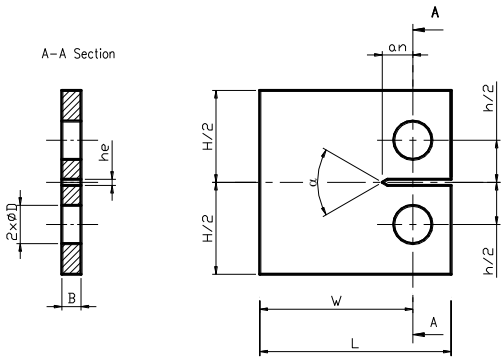

Fig. 2 – Geometry of the CT specimens.

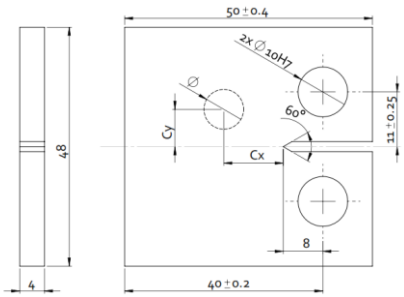

Fig. 3 – Modified CT specimens made of S235 steel grade.

Tab. 4 – Dimensions of the CT specimens.

Material	W mm	B mm	L mm	H mm	h mm
S235*	50	4	50	48	22
S355*	40	4	50	48	22
S355**	50	8	62.5	60	27.5
S690**	40	5	50	48	22

Material	D mm	h_e mm	a_n mm	α °
S235*	10	1.7	8	60
S355*	10	1.7	8	60
S355**	12.5	3	10	60
S690**	10	1.6	8	60

*Tested in this study
**Tested by De Jesus *et al.* (2012)

During tests, cracks were measured on both side faces of the CT specimens, by direct observation through a magnification system (resolution of 1 μm). The crack propagation tests were performed under load control and with a frequency of 20 Hz, which was reduced as soon as the crack achieved high crack growth rates (approximately 0.3 mm/1000 cycles). Two stress ratios were covered by the tests performed in this work, namely R_σ=0.01 and R_σ=0.5. Table 5 and Table 6 summarize the testing conditions that were followed for the fatigue crack propagation tests performed in this work.

Tab. 5 – Summary of fatigue crack growth tests performed on S235 steel.

Specimens	R_σ	Mode	Hole Coord. mm	ϕd mm	ΔK_{ini} Nmm
S235_01_01	0.01	I	-	-	474.3
S235_01_02	0.01	I	-	-	474.3
S235_05_01	0.50	I	-	-	474.3
S235_05_02	0.50	I	-	-	474.3
S235_I+II_01_01	0.01	I+II	C_x=12 / C_y=7.5	7.0	474.34
S235_I+II_01_02	0.01	I+II	C_x=12 / C_y=7.5	7.0	474.34
S235_I+II_01_03	0.01	I+II	C_x=12 / C_y=8.0	7.5	474.
S235_I+II__01_04	0.01	I+II	C_x=10 / C_y=7.0	7.5	474.
S235_I+II__01_05	0.01	I+II	C_x=10 / C_y=7.0	7.5	474.

Tab. 6 – Summary of the fatigue crack growth tests performed on S355 steel.

Specimens	R_σ	B mm	$\Delta K_{initial}$ Nmm$^{1.5}$
S355_T4_01_01	0.01	4	474.34
S355_T4_01_02	0.01	4	474.34
S355_T4_05_01	0.50	4	474.34
S355_T4_05_02	0.50	4	474.34
S355_T8_01_01	0.01	8	474.34
S355_T8_01_02	0.01	8	474.34
S355_T8_05_01	0.50	8	474.34
S355_T8_05_02	0.50	8	474.34

4. RESULTS AND DISCUSSION

4.1. Cyclic elastoplastic behaviour

In this section the cyclic elastoplastic behaviours of the S235 and S355 steels are presented based on results from the tests performed in this research. The first results to be presented are the evolution of the cyclic stress amplitude with the number of cycles. Since tests were performed under strain controlled conditions, these results clarify the cyclic hardening/softening behaviour of the materials. These results are presented in Figs. 4 and 5, respectively for the S235 and S355 steels. Figs. 6 and 7 presents the hysteresis loops obtained for half-life, respectively for S235 and S355 materials.

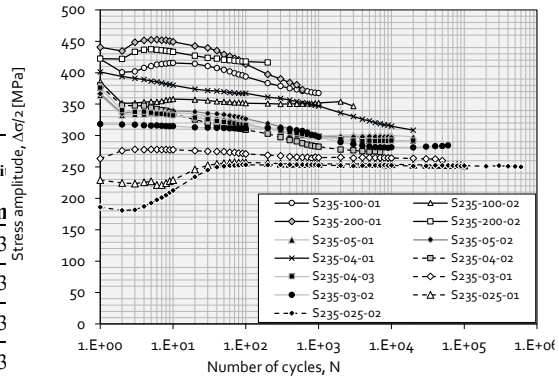

Fig. 4 – Stress amplitude versus number of cycles to failure obtained for the S235 steel.

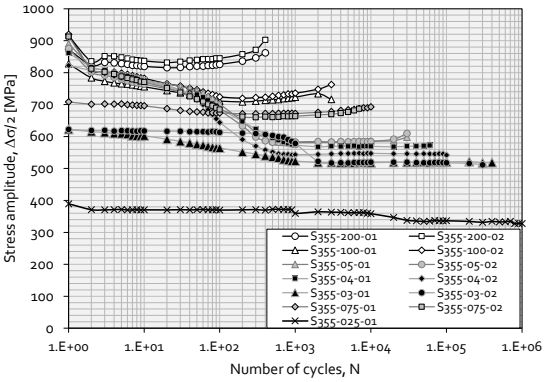

Fig. 5 – Stress amplitude versus number of cycles to failure obtained for the S355 steel.

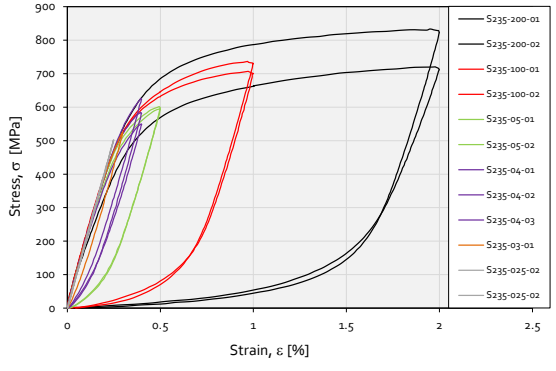

Fig. 6 – Half-life hysteresis loops of the S235 steel.

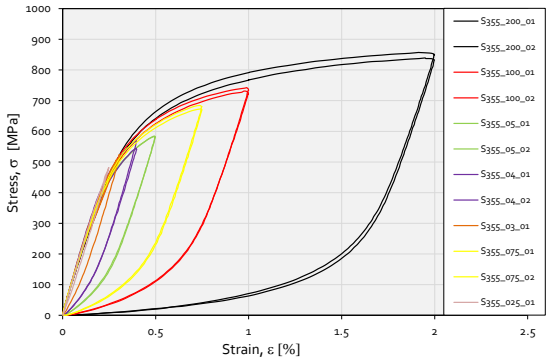

Fig. 7 – Half-life hysteresis loops of the S355 steel.

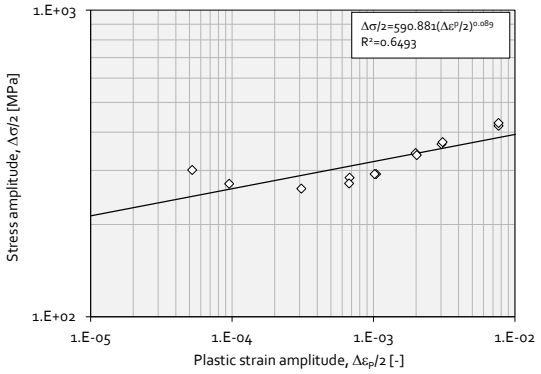

Fig. 9 – Cyclic curve of the S355 steel.

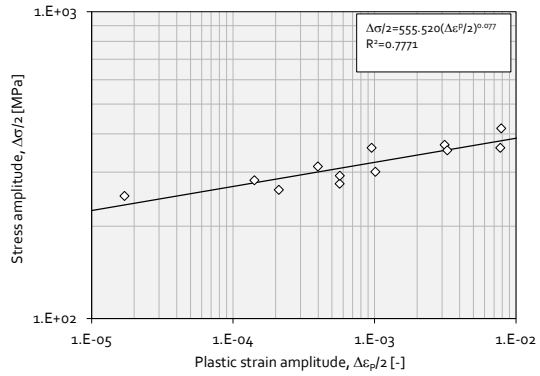

Fig. 8 – Cyclic curve of the S235 steel.

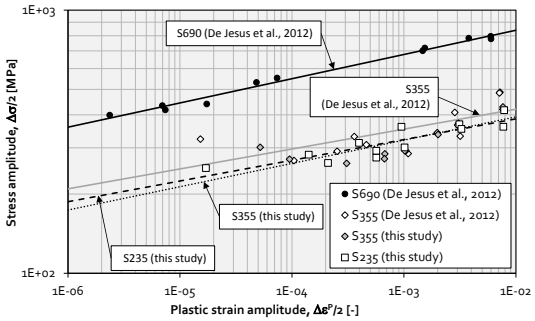

Fig. 10 – Comparison of cyclic curves obtained for S690, S355 and S235 steel grades.

Figs. 8 and 9 illustrate the cyclic stress-strain curves obtained for the S235 and S355 steels, respectively. Fig. 10 shows a comparison of the cyclic curves between the S690, S355 and S235 steels.

The S235 steel exhibits, under cyclic elastoplastic conditions, a general cyclic softening trend. The S355 steel shows a general stabilized cyclic behaviour with some visible exceptions of cyclic softening. This mixed stabilized/softening behaviour was also confirmed by De Jesus *et al.* (2012) for the S355 steel, using an independent testing campaign on the S355 steel (see Fig. 11a). Fig. 11b) shows the cyclic stress amplitude versus cycles obtained for the S690 steel by De Jesus *et al.* (2012). We observe that this material shows a quasi-stabilized cyclic behaviour just after the first cycles. Only small amounts of cyclic hardening is observed for high strain ranges (Δε>1%). In general, we may conclude that the stabilized cyclic conditions increase with increasing static strength of the structural steels.

The analysis of the hysteresis loops of the tested steels shows some scatter in the results.

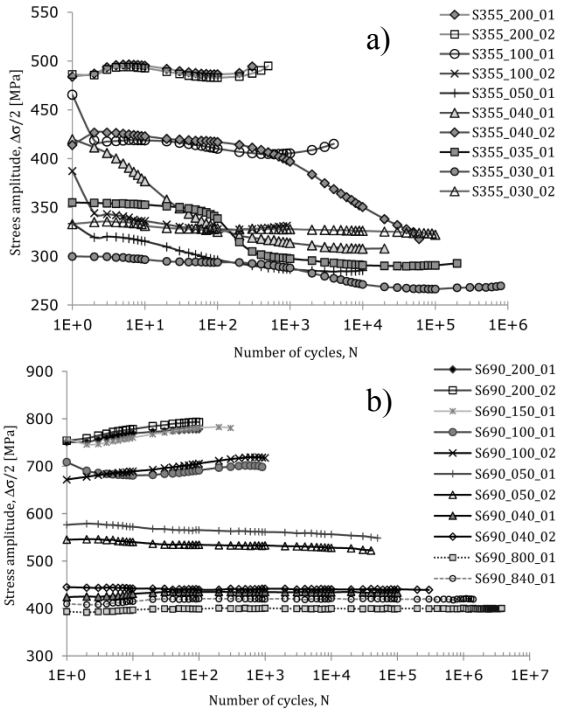

Fig. 11 – Stress amplitude versus number of cycles to failure obtained by De Jesus *et al.* (2012): a) S355 steel; b) S690 steel.

This scatter results in some deviations from the Masing behaviour of the materials. The cyclic curves of the steels presented in Figs. 8 and 9 show moderate determination

coefficients. Fig. 10 compares the cyclic curves obtained for the S235, S355 and S690 steels. Taking into account the scatter observed in the experimental results that were used to compute the cyclic curve of the materials, the S235 and S355 steels – both mild steels – show very similar cyclic curves. The S690 steel shows a significantly distinct cyclic curve (higher cyclic yield strength), almost parallel to the ones of the other steels, in the log-log representation.

4.2. Strain-life behaviour

This section presents the strain life results and its analysis covering the three structural steels under investigation. Figs. 12 and 13 present the total strain-life relations obtained, respectively, for the S235 and S355 steels, tested in this investigation. The experimental data was correlated using the Basquin, Coffin-Manson and Morrow relations (see Eqs. (1) to (3)).

Figs. 14, 15 and 16 compare the strain-life curves obtained for the materials tested in this study and also for the materials tested by De Jesus *et al.* (2012). The analysis of Figs. 14 and 15 shows that a significant difference is found between the high strength and the mild steels. The differences in the fatigue behaviours between the S235 and S355 steels may not be statistically representative, given the observed scatter in the experimental data. The S690 steel shows higher fatigue strength (see Fig. 15) and lower fatigue ductility (see Fig. 14) than mild steels. The comparison of the global strain-life relations presented in Fig. 16 shows interesting results: i) for low-cycle fatigue, the S690 steel shows lower fatigue resistance than mild steels; ii) for high-cycle fatigue the S690 steel shows higher fatigue resistance than mild steels; iii) the S235 and S355 mild steels show very similar results; iv) the S355 steel tested in this study and by De Jesus *et al.* (2012) have almost coincident behaviours showing the reproducibility of the results even using distinct material batches; v) the strain-life curves rotate about a point corresponding to 6E3–2E4 cycles. With respect the S690 curve, there is a clockwise rotation whose rotate value increases with the decrease in the material static strength.

Table 7 summarizes the cyclic constants

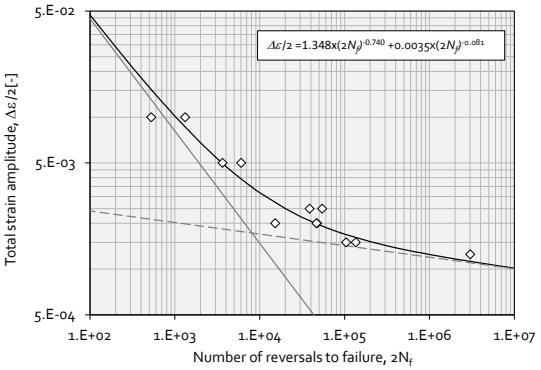

Fig. 12 – Strain-life data for the S235 steel grade.

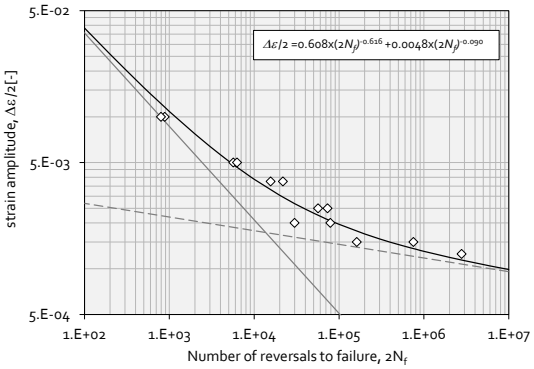

Fig. 13 – Strain-life data for the S355 steel grade.

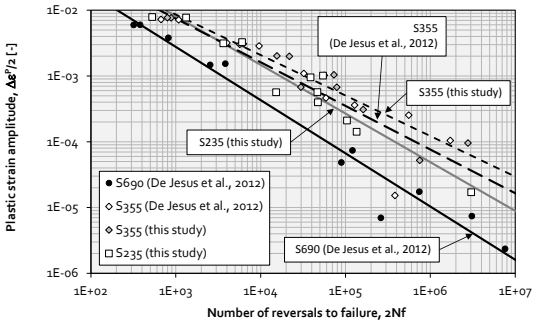

Fig. 14 – Comparison of plastic strain-life data between the S235, S355 and S690 steels.

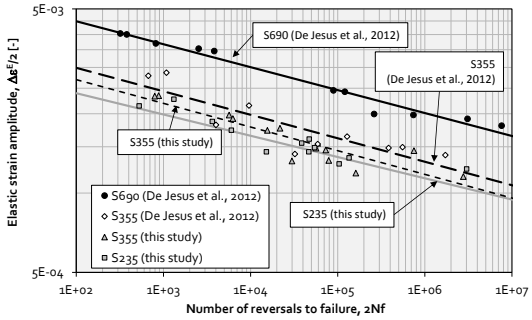

Fig. 15 – Comparison of elastic strain-life data between the S235, S355 and S690 steels.

of the materials tested in this work and tested by De Jesus *et al.* (2012). One may conclude

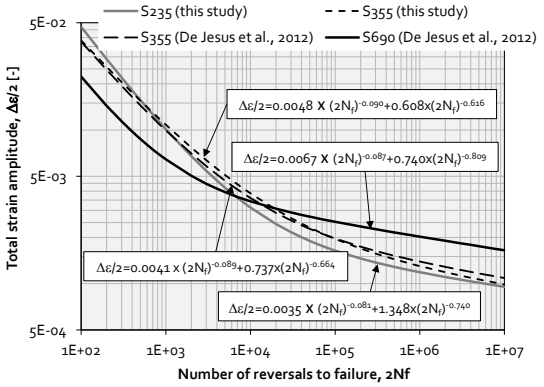

Fig. 16 – Comparison of strain-life data between the S235, S355 and S690 steels.

Tab. 7 – Summary of cyclic elastoplastic and fatigue constants.

Steel grade	K'	n'	σ_f'/E	b	ε_f'	c	$2N_T$
	[MPa]	[-]	[MPa]	[-]	[-]	[-]	
S235 (this study)	555.5	0.079	0.0035	-0.081	1.348	-0.740	6822
S355 (this study)	590.9	0.089	0.0048	-0.090	0.608	-0.616	4054
S355 (De Jesus *et al.*, 2012)	595.9	0.076	0.0041	-0.089	0.737	-0.664	7095
S690 (De Jesus *et al.*, 2012)	1282	0.092	0.0067	-0.087	0.740	-0.809	675

that besides the significantly higher strain hardening coefficient, the S690 steel shows very low number of transition reversals between the strength dominated fatigue behaviour and the ductility dominated fatigue behaviour.

4.3. Pure mode I fatigue crack growth rates

This section presents the fatigue crack growth rates obtained in this study for the S235 and S355 steels. Also, similar data derived by De Jesus *et al.* (2012) for the S355 and S690 steels are presented for comparison purposes. Fig. 17 presents the fatigue crack propagation data obtained for the S355 steel tested using CT specimens with a thickness of 4 mm and covering two stress ratios, namely R_σ=0.01 and R_σ=0.5. The data was correlated using the Paris law. A very small influence of the stress ratio on fatigue crack propagation rates was observed.

Fig. 18 presents the fatigue crack propagation rates for the S355 steel tested with a thickness of 8 mm. For this case, a slightly higher stress ratio influence is observed than verified for the thickness of 4 mm. Fig. 19 plots

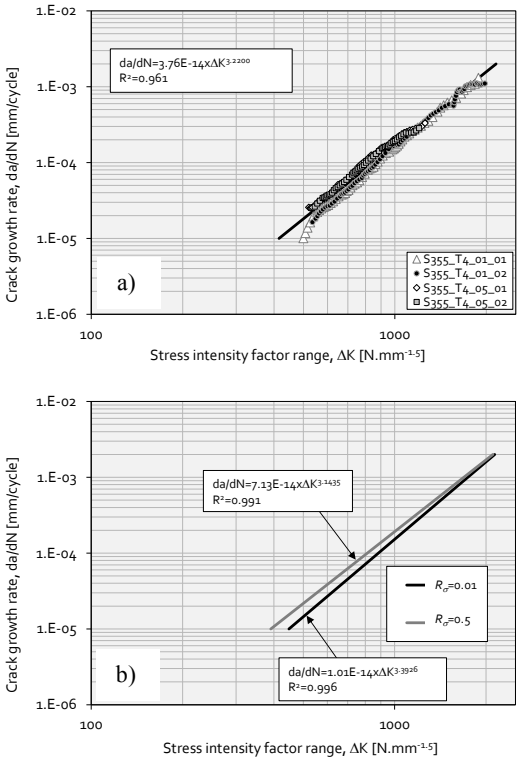

Fig. 17 – Fatigue crack propagation rates obtained for the S355 steel, for a thickness of 4mm: a) global correlation of experimental data for R_σ=0.01 and R_σ=0.5 joined together; b) comparison of regression lines for each stress ratio.

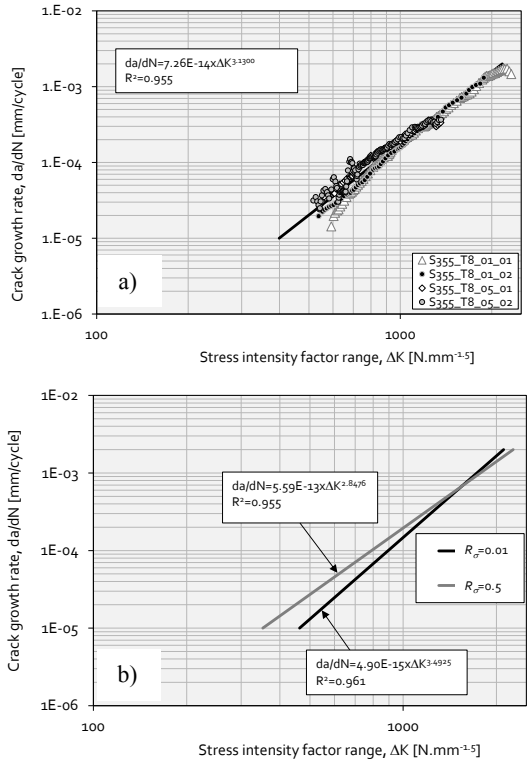

Fig. 18 – Fatigue crack propagation rates obtained for the S355 steel, for a thickness of 8 mm: a) global correlation of experimental data for R_σ=0.01 and R_σ=0.5 joined together; b) comparison of regression lines for each stress ratio.

all the data derived for the S355 steel (both thicknesses and stress ratios). In Fig. 19a) all data was correlated with the Paris law and a significant determination coefficient was observed. However, it was possible to increase this determination coefficient using the effective stress intensity factor as proposed by Walker (1970). This effective stress intensity factor is suitable for modelling the mean stress effects in this material. Fig. 20 compares the fatigue crack propagation rates obtained in this study for the S355 steel grade, for thicknesses equal to 4 and 8 mm with the fatigue crack propagation rates obtained by Albuquerque *et al.* (2012) for the same material with a thickness of 30 mm. One may conclude that the thickness has a negligible influence on fatigue crack propagation results between until 30 mm.

Fig. 21 presents the fatigue crack propagation data obtained in this study for the S235 steel. For this steel, only the stress ratio effects were assessed. However, and despite a small increase in the fatigue crack propagation rates with the stress ratio, this

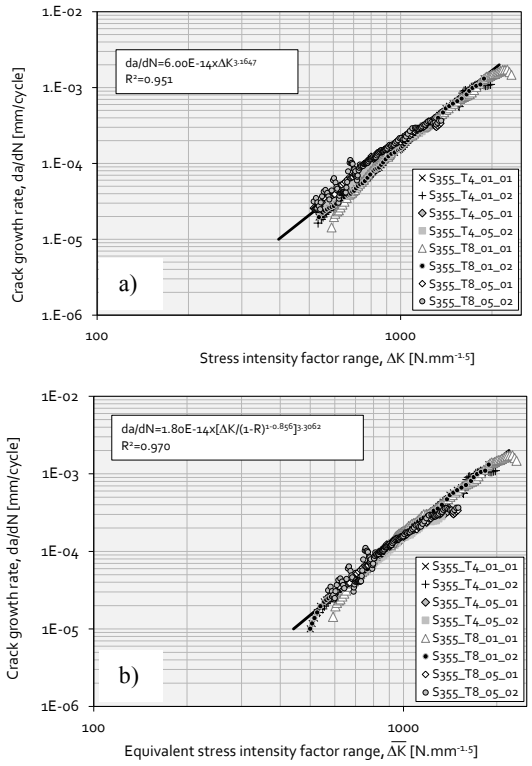

Fig. 19 – Fatigue crack propagation rates obtained for the S355 steel: a) global correlation of experimental data using Paris relation; b) global correlation of experimental data using Walker relation.

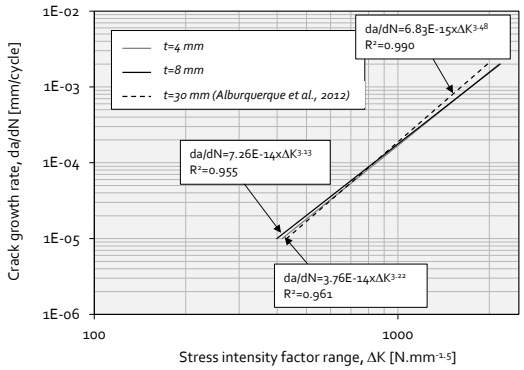

Fig. 20 – Fatigue crack propagation rates obtained for the S355 steel: thickness influence.

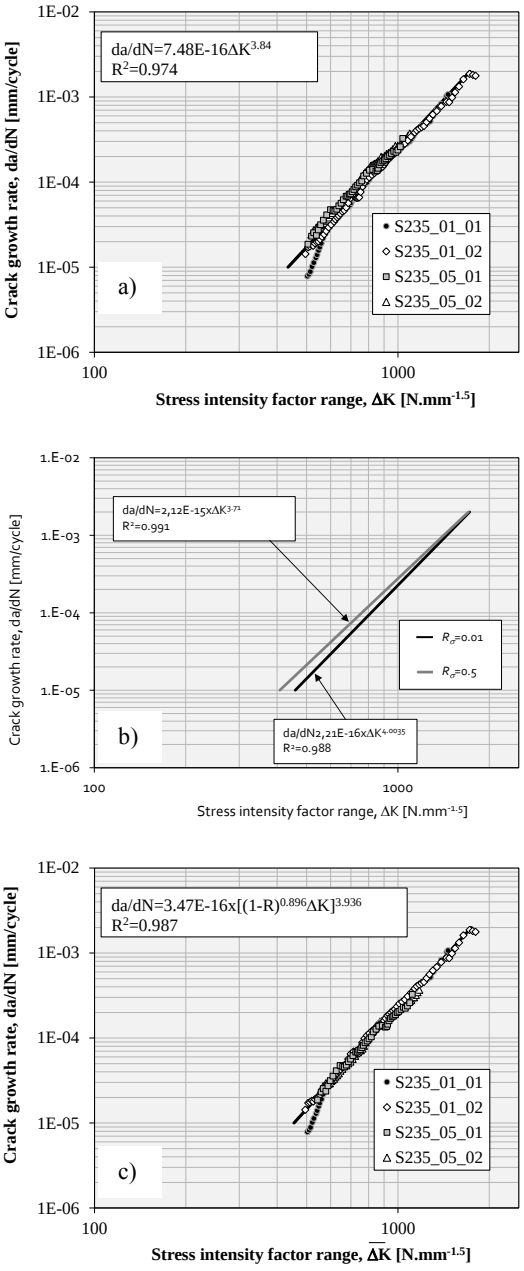

Fig. 21 – Pure mode I fatigue crack propagation rates obtained for the S235 steel: a) correlation of all data with the Paris law; b) comparison of Paris regression lines for each stress ratio; c) correlation of all data using Walker model.

effect is considered to be minor. Fig. 21c shows the correlation of the mode I fatigue crack propagation rates obtained for the S235 steel using the Walker model which resulted in the increase of the determination coefficient, in comparison with the one obtained with the Paris relation.

Fig. 22 compares the global fatigue crack propagation trends obtained for the S235, S355 and S690 steels, tested in this study and tested by De Jesus *et al.* (2012). One interesting observation is the clear higher fatigue crack propagation rates observed for the S690 steel, independently of the stress ratio. With respect to the S355 and S235 steels, the comparison of their crack propagation rates is not so clear since contradictory results may be observed. For example, for R_σ=0.01, the S235 shows higher fatigue crack propagation rates than S355 steel; however for R_σ=0.5 the S235 steel shows higher fatigue crack propagation rates than S355 steel tested in this study, but lower values than S355 steel tested by De Jesus *et al.* (2012). However, the differences between fatigue crack propagation rates for these two steels are lower than the one obtained for the S690 steel. Another important aspect is the stress ratio influence that is higher for the S690 steel than for the mild steels.

4.4. Mixed mode I+II fatigue crack growth rates for S235 steel

In addition to the pure mode I fatigue crack propagation tests, the S235 steel was further tested under mixed I+II mode conditions. For this purpose, a modified CT specimen was used with a side circular hole, as represented in Fig. 3. The position of the

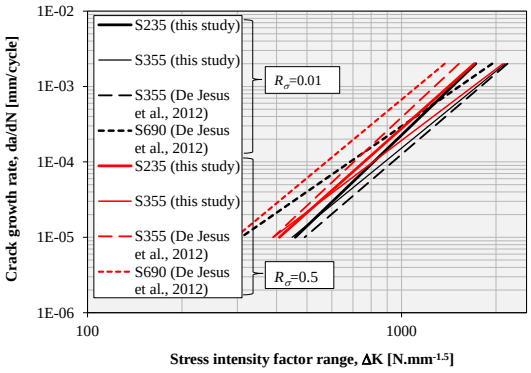

Fig. 22 – Comparison of fatigue crack propagation rates between the S235, S355 and S690 steels.

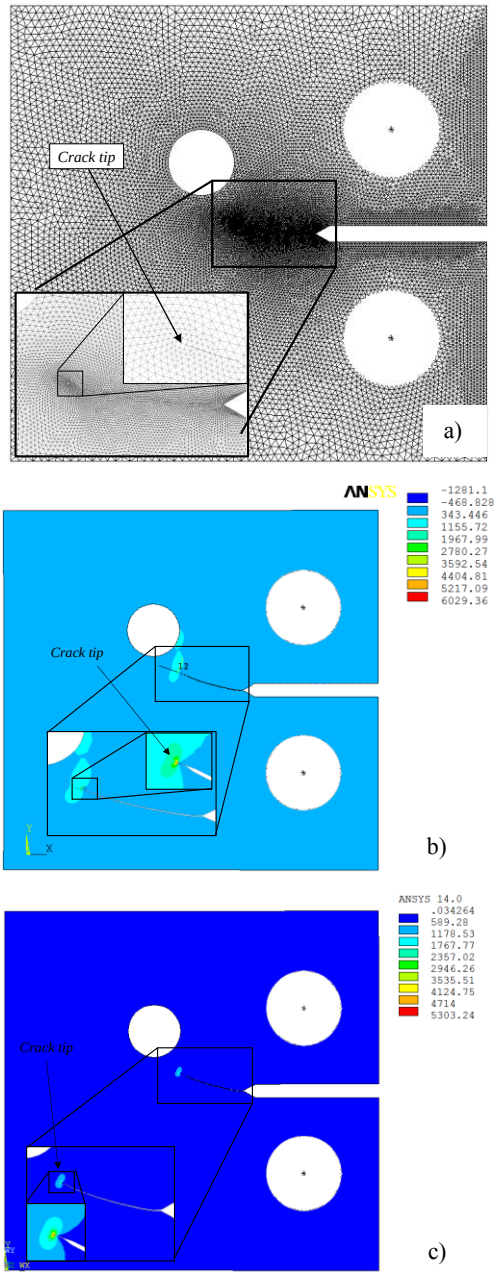

Fig. 23 – Finite element modelling of a mixed-mode CT specimen: a) finite element mesh; b) direct stress field results according loading direction; c) direct stress field results along the transverse direction for crack tip frame.

side hole was parameterised to produce distinct mixed mode conditions. The observed crack paths were simulated by the finite element method. Fig. 23 illustrates results for a particular case and crack increment. Using the Virtual Crack Closure Technique (Krueger, 2004), mode I and mode II stress intensity factors were computed. An equivalent stress intensity factor was then computed using the relation proposed by Tanaka (1974):

$$\Delta K_{eq} = \sqrt[4]{\Delta K_I^4 + 8\Delta K_{II}^4} \quad (7)$$

Fig. 24a) plots the fatigue crack propagation rates obtained with the mixed-mode tests. The fatigue crack growth rates were plotted against the equivalent stress intensity factor ranges. The data was correlated using the Paris relation and a good determination coefficient was obtained. Fig. 24b) plots the fatigue crack growth rates for both pure mode I and mixed I+II mode fatigue crack propagation rates. One may observe that Paris relation still correlates the data with a high determination coefficient.

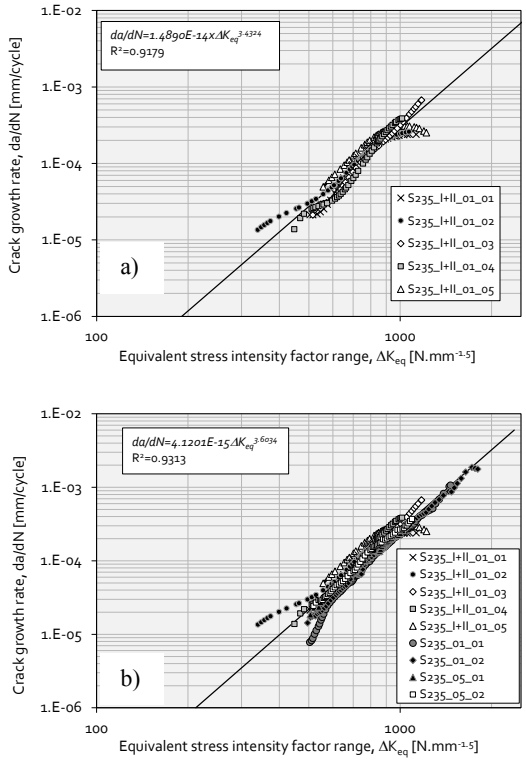

Fig. 24 – Mixed-mode fatigue crack propagation rates obtained for the S235 steel: a) correlation of mixed-mode I+II data; b) correlation of mixed-mode plus pure mode I fatigue data.

5. CONCLUSIONS

A comparison of the fatigue behaviour between three structural steels was presented, namely between S235, S355 and S690 steels. The S235 and S355 steels are considered mild steels, while the S690 steel is considered a high strength steel. Fatigue results based on smooth specimens were used in this comparison as well as fatigue crack propagation tests. The following conclusions may be formulated:

- Taking into account the scatter of fatigue test results, the two investigated mild steels shows similar fatigue properties.
- There is a clear distinction between the fatigue performance of the high strength and mild steels.
- The mild steels show lower fatigue crack propagation rates than the high strength steel.
- The strain-life curve suffers a clock-wise rotation with the decrease of the steel static strength. This result makes the high strength steels more fatigue resistant for low-cycle fatigue.
- Stress ratio effects were more relevant for the high strength steel than for the mild steels.

Besides the comparison between materials, some particular conclusions concerning the S235 and S355 steels may be formulated. Concerning the S355 steel, it was observed no thickness influence on fatigue crack propagation rates for thicknesses between 4 and 30 mm. Concerning the S235 steel, mixed-mode fatigue crack propagation data were highly correlated with pure mode I fatigue crack propagation data for this steel.

ACKNOWLEGMENTS

The authors acknowledge the Fundação para a Ciência e Tecnologia for their financial support through the SFRH/BD/72434/2010 grant.

REFERENCES

Albuquerque, C. M. C., Miranda, R., Richter-Trummer, V., Figueiredo, M., Calçada, R., De Castro, P. M. S. T. 2012. Fatigue crack propagation behaviour in thick steel weldments, International Journal of Structural Integrity, 3(2), p. 184 – 203.

De Jesus, A.M.P., Matos, R., Fontoura F. and Veljkovic, M. 2012. A comparison of the fatigue behavior between S355 and S690 steel grades, Journal of Constructional Steel Research, 79 , p. 140–150.

ASTM, 1998. ASTM E606: Standard Practice for Strain-Controlled Fatigue Testing, In: Annual Book of ASTM Standards, Vol. 03.01, ASTM - American Society for Testing and Materials, West Conshohocken, PA, USA.

ASTM, 1999. E647: Standard Test Method for Measurement of Fatigue Crack Growth Rates, In: Annual Book of ASTM Standards, Vol. 03.01, ASTM - American Society for Testing and Materials, West Conshohocken, PA, USA.

Basquin, O.H. 1910. The exponential law of endurance tests". Proc. Annual Meeting, American Society for Testing Materials, 10, p. 625-630.

CEN, 2003. EN 1993-1-9: Eurocode 3, Design of steel structures – Part 1-9: Fatigue, CEN-TC 250, European Committee for Standardization, Brussels.

CEN, 2004. EN 10025: hot rolled products of structural steels. European Committee for Standardization. Brussels: European Standard.

Chen, H., Grondin G.Y., Driver, R.G. 2005 Fatigue resistance of high performance steel. Structural engineering report no 258. Canada: University of Alberta.

Chen, H., Grondin, G.Y., Driver, R.G. 2007. Characterization of fatigue properties of ASTM A709 high performance steel. Journal of Constructional Steel Research, 63, p.838-848.

Coffin, L.-F. 1954. A study of the effects of the cyclic thermal stresses on a ductile metal, Translations of the ASME, 76, p.931–950.

Krueger, R. 2004. Virtual crack closure technique: History, approach, and applications, Applied Mechanics Reviews, 57(2), p.109-143.

Manson, S.S. 1954. Behaviour of materials under conditions of thermal stress. NACA TN-2933, National Advisory Committee for Aeronautics.

Morrow, J.D. 1965. Cyclic plastic strain energy and fatigue of metals, International Friction, Damping and Cyclic Plasticity, ASTM, STP 378, p. 45-87.

Paris, P. Erdogan, F. 1963. A critical analysis of crack propagation laws, Journal of Basic Engineering, 85, p. 528-534.

Ramberg, W., Osgood, W.R. 1943. Description of stress–strain curves by three parameters, NACA TN-902. USA: National Advisory Committee for Aeronautics.

Tanaka, K. 1974, Fatigue Crack propagation from crack inclined to the cycle tensile axis, Engineering Fracture Mechanics, 6, p. 496-507.

Walker, EK. 1970. The effect of stress ratio during crack propagation and fatigue for 2024-T3 and 7076-T6 aluminum. In: Effect of environment and complex load history on fatigue life, ASTM STP 462. Philadelphia: American Society for Testing and Materials, p.1–14.